



# Rainfall variability and its teleconnection with atmospheric circulation anomalies over southern and southeastern region, Ethiopia

Tewelde Berihu<sup>1,2,3</sup> · Wen Chen<sup>1,4</sup> · Lin Wang<sup>5</sup>

Received: 24 November 2023 / Accepted: 27 March 2024 / Published online: 25 April 2024  
© The Author(s), under exclusive licence to Springer-Verlag GmbH Austria, part of Springer Nature 2024

## Abstract

Factors related to rainfall variabilities in southern and southeastern Ethiopia have not yet been addressed. The extreme wet and dry events caused by atmospheric circulation patterns during the March–April–May periods were studied using 1991–2022 data from Climate Hazard Group InfraRed Precipitation with Stations (CHIRPS) and atmospheric circulation anomalies datasets. Empirical orthogonal function (EOF), precipitation concentration index (PCI), and coefficient of variation (CV) are used to determine the interannual variation. The study revealed that both PCI and CV exhibit rainfall variability with increasing magnitude from west to east of the region, while the first mode of EOF showed a dominantly uniform pattern and accounted for 48.8% of the observed variance. Eight extreme dry and four extreme wet years were also observed. Composite analyses suggested that the study area during wet years were characterized by convergence or divergence of velocity potential, and decrease or increase of vertical velocity at lower or upper troposphere which favorable conditions to vertical motion, while opposite phenomena observed during dry periods. Westerly winds from the southern Atlantic Ocean were associating with wet, while easterly winds from the Indian Ocean with dry. The study found a negative correlation between rainfall and Azores SLP, a positive correlation with Indian Ocean SST, and 62.5% of the driest periods coexisted with La Niña events. In summary, Indian Ocean SST, Nino Index 3.4, Azores SLP, South Atlantic 850-hPa westerly winds, and vertical velocity are predictive factors that should be considered in the rainfall forecasting process in the study area.

✉ Tewelde Berihu  
tewelde@mail.iap.ac.cn  
Wen Chen  
chenwen-dq@ynu.edu.cn  
Lin Wang  
linwang@mail.iap.ac.cn

- <sup>1</sup> Center for Monsoon System Research, Institute of Atmospheric Physics, Chinese Academy of Sciences, Beijing, China
- <sup>2</sup> Colleges of Earth and Planetary Sciences, University of Chinese Academy of Sciences, Beijing, China
- <sup>3</sup> Meteorology and Hydrology, Arba Minch University, P.O. Box 21, Arba Minch, Ethiopia
- <sup>4</sup> Departments of Atmospheric Sciences, Yunnan University, Kunming 650500, China
- <sup>5</sup> CAS Key Laboratory of Regional Climate-Environment for Temperate East Asia, Institute of Atmospheric Physics, Chinese Academy of Sciences, Beijing 100029, China

## 1 Introduction

Rainfall is both a fundamental parameter of the hydrological cycle and a climate variable, playing an important role in agricultural production (Cheung et al. 2008) and water resource management (Barua et al. 2013) for local, regional, and global scales. It is also input to streamflow for hydropower generation (Beheshti et al. 2019) to improve the socio-economics of a nation. The magnitude of rainfall and its distribution is crucial for sustainable food security, especially for developing countries such as Ethiopia. As indicated by Cheung et al. (2008), the failure to maintain a consistent rainfall supply in terms of time and quantity leads to food insecurity. Literature (Seyoum et al. 2015; Teshome and Lupi 2018) shows that Ethiopia's main source of national economy is agriculture, which accounts for 40% of GDP, 80% of total employment, and 90% of exports. The

agricultural sector is sensitive to extreme weather and is mainly affected by rainfall variability. The rainfall variabilities have seriously affected the country's economic growth, leading to a 10% decrease in its gross domestic product (Gebremichael et al. 2014). Research conducted by (Gum-madi et al. 2018) in Ethiopia analyzed the rainfall variability and found that the temporal coefficient variation (CV,%) of rainfall was 9–30% in annual, 9–69% in summer, and 15–55% in spring. Further study Abegaz (2020) in central Ethiopia also found high rainfall variations both in space and time.

The two extremes rainfall aspects (drought and flood) are common climatic disasters in Ethiopia and cause economic losses. For example, the drought caused by El Niño in 2015/2016 affected approximately 10 million people making it one of the highest recorded droughts (A. Teshome & Zhang, 2019) and five million people in 2017 (H. Tes-home et al. 2022). Most of the time drought in Ethiopia is caused by chronic deficiency of rainfall for one season or extended periods (Mekonnen 2020). As cited by Mekonen et al. (2020), the frequency of drought (failure of rainy season) has been increasing from once every decade before the 1970s and 1980s, to twice every three years from 1980 to 2004 and then once a year until 2011. Similarly, floods are also the second aspect of extreme excessive rainfall events, which are common in different regions of the country, such as eastern Ethiopia (Semie et al. 2023) & (Billi et al. 2015) and southwestern Ethiopia (Haile et al. 2013).

Previous studies have shown that extreme rainfall variabilities (dry and rainy seasons) are related to global and regional large-scale atmospheric-ocean circulation, such as sea surface temperature anomalies (Patil & Doi, 2023), El-Niño Southern Oscillation (ENSO) and Indian Ocean Dipole (IOD) (Jayakumar 2021; Kebacho 2022), Madden–Julian Oscillation (Finney et al. 2020), Tropical easterly jet stream that triggered by global sea surface temperature (Manatsa et al. 2008). As indicated by Segele et al. (2009), Ethiopian summer rainfall is suppressed during El Nino and enhanced during La Nina. However, these studies and other related literature (Alhamsry et al. 2020; Diro et al. 2011) have attempted to link local seasonal rainfall to global sea surface temperatures and there is still a lack of knowledge of the influence of atmospheric dynamics such as wind anomalies, vertical velocity and other atmospheric variables on the local rainfall, especially in the study area.

The impact of these remote teleconnections, such as tropical sea surface temperature anomalies and semi-permanent pressure centers, and their association with atmospheric dynamics, vary seasonally and regionally and should therefore be studied separately. This study was focused on spring (March–April–May) in southern and southeastern Ethiopia. As shown by Degefu et al. (2021) and Viste et al. (2013),

rainfall in these areas has decreased and drought incidence has increased.

Therefore, this study aimed to analyze rainfall variability, identify surplus and deficit periods, and link them with atmospheric-ocean variables from 1991 to 2022. We used the coefficient of rainfall variation (CV), precipitation concentration index (PCI), empirical orthogonal function (EOF), student t-test, and composite and correlation analyses to achieve these objectives.

Characterized rainfall of past abnormal rainfall events and abnormal atmospheric circulation anomalies can help formulate strategies and policy mechanisms to minimize their impact on agricultural production and provide predictive factors for rainfall forecast operations.

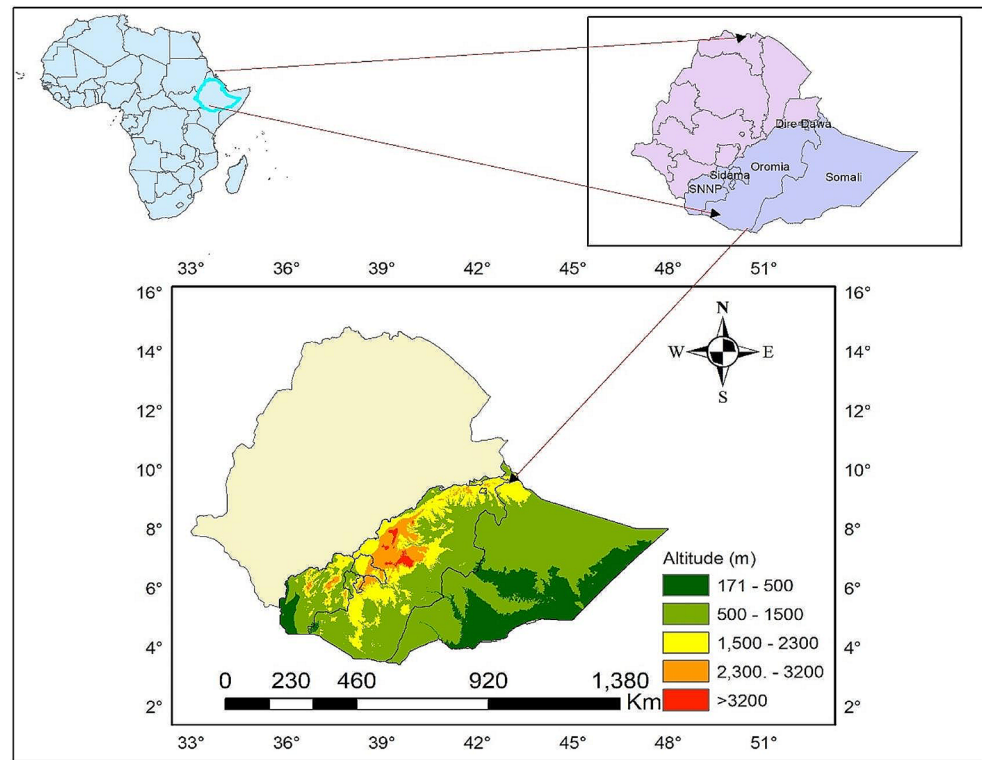
The structure of this article is divided into the following sections: the first section introduces an overview of the background information of the title, the second section describes the data and methods, and the third section provides the results and discussion. Finally, sect. 4 presents the summery and conclusions drawn from the research results.

## 1.1 Data and methods

The overall approaches of this study consist of two main tasks: We first analysed the rainfall variability over the March–April–May seasonal time series using the methods of precipitation concentration index (PCI), coefficient of variation (CV), and empirical orthogonal function (EOF/PCA). The second task involves identifying the most dry and wet extreme seasonal rainfall over time domain (1991–2022) using principal components (PC1), then, associating to atmospheric circulation patterns using composite analysis to reveal the underlying possible mechanisms related to the key dry and wet conditions.

## 1.2 Description of the study area

Ethiopia is one of the East African countries that geographically runs from 3° to 15°N and 33° to 48°E with a total surface area of about 1.1 million square kilometers. It is bordered by Kenya to the south, Somalia to the east, Sudan to the northwest, South Sudan to the southwest, Eritrea to the north, and Djibouti to the northeast. Ethiopia is renowned for its ecological diversity from tropical to temperate regions. The altitude ranges from 126 m in the northeast of the Danakil Depression to 4620 m in the northwest of the Ras-Dashen Mountains (Ayalew 2020). The study area covers the southern and southeast regions of the country which geographically runs from 3° to 9°N and 33° to 48°E as shown in (Fig. 1). It includes Majority of Somali regional state, Sidama, some portion of southern national nationality and people (SNNP) and South Oromia regional state.

**Fig. 1** The study area

Altitude is one of the elements that used to climate zoning tool (Weldegerima et al. 2023) and the study area ranges from low land (less than 500 m) to upper highland areas (greater than 3200 m) as shown in (Fig. 1). The boundary shape file of the study area is taken from the global administration database found in the link [https://gadm.org/download\\_country.html](https://gadm.org/download_country.html).

Rainfall regimes in Ethiopia are heterogeneous due to complex topography, and various authors have attempted zoning in different homogeneous clusters (Gleixner et al. 2017). The most dominant areas of southern and south-eastern Ethiopia are bimodal, with March–April–May being a major rainy season and September–October–November being a second rainy season (Link et al. 2020). This seasonal cycle is caused by the migration of the Inter-Tropical Convergence Zone (ITCZ) (Nicholson 2018).

Spring (February/March to May) is also the second rainy season for the areas of Sidama (Matewos and Tefera 2020), Arsi (Mekonnen et al. 2018), West Arsi (Senbeta 2009), West and East Hararrge (IGAD 2017) and Bale High lands (Legese Jima et al. 2019) which are parts of this study domain. The geographical and seasonal scope of this study focuses on the second and first spring rainfall areas from March -April- May (see Fig. 1).

### 1.3 Satellite-gauge merged rainfall products

Four groups of rainfall products are currently available (Adnew et al. 2022) and they are gauged interpolated, satellite only, satellite-gauge merged, and reanalysis products. For incomplete historical rainfall time series and rain gauge areas with low density such as Ethiopia, satellite rainfall products are the best choice to fill this gap and have been applied in different regions (de Moraes Cordeiro & Blanco, 2021; Hordofa et al. 2021; Perera et al. 2022). In this study, satellite and measurement product type Climate Hazard Center InfraRed Precipitation Station (CHIRPS) datasets were used for rainfall variability analysis. It is developed by the U.S. Geological Survey (USGS) and the University of California Climate Hazards Group (CHG) (Bayissa et al. 2017).

This satellite dataset has advantages to being selected because of sufficient time series length, fine resolution, and free access for international researchers. Furthermore, a study Dinku et al. (2018) conducted in East Africa found that CHIRPS was significantly better than the other four satellite rainfall products at a monthly time scale. In a similar study that was conducted in Ethiopia (Gebremicael et al. 2017), CHIRPS shows more agreement with the observed among the other eight satellite estimates. Therefore, CHIRPS is the best choice used in this study.

## 1.4 Data for atmospheric circulation anomalies

Atmospheric data used in this study include zonal ( $u$ ) and meridional ( $v$ ) wind components and vertical velocity for the period 1991–2022. These datasets were obtained and extracted from the European Center Medium-Range Weather Forecast (ECMWF) ERA-5 version with a spatial resolution of  $0.25^\circ \times 0.25^\circ$ . It is free to access online database (Hua et al. 2019). Several authors (Fu et al. 2022; Manjowe et al. 2018; Raveh-Rubin and Wernli 2015) have used these reanalysis datasets to explore the association between large-scale circulation and rainfall variabilities. The El Niño-Southern Oscillation (ENSO) dataset for spring (MAM) was obtained from the National Oceanic and Atmospheric Administration website at the link:

[https://origin.cpc.ncep.noaa.gov/products/analysis\\_monitoring/ensostuff/ONI\\_v5.php](https://origin.cpc.ncep.noaa.gov/products/analysis_monitoring/ensostuff/ONI_v5.php).

Sea surface temperature (SST) with  $1^\circ \times 1^\circ$  horizontal resolution, sea surface pressure (SLP) with  $(2.5^\circ \times 2.5^\circ)$ , and velocity potential with  $(2.5^\circ \times 2.5^\circ)$  data were used from the National Center of Environmental Prediction (NCEP) reanalysis (Kalnay et al. 1996).

## 2 Methods

The temporal and spatial variability of rainfall was analyzed at the rainy seasons.

(March-April-May) time scale. The methods engaged in this study are coefficient of variation (CV), precipitation concentration index (PCI), and Empirical orthogonal function (EOF/PCA).

### 2.1 Coefficient of variation (CV)

CV is used to class the grade of rainfall variability and it is employed in this study to assess the rainfall characteristics for the March-April-May time scale. CV is widely applicable and the computation of its value with a degree of variability (Bayable et al. 2021) is given below:

$$CV = \frac{\sigma}{\mu} \times 100 \quad (1)$$

The class of rainfall variability is categorized as high ( $CV > 30$ ), moderate ( $20 < CV < 30$ ), and low ( $CV < 20$ ). Therefore, the highest value of CV indicates higher variability of rainfall and the lowest value of CV indicates uniform distribution,  $\mu$  mean of rainfall, and  $\sigma$  standard deviation of rainfall.

### 2.2 Precipitation concentration index (PCI)

PCI is one of the methods used to evaluate the rainfall distribution as applied by (AL-Shamarti 2016; Silva et al. 2022; Zhang et al. 2019). According to Oliver (1980) the equation of PCI presents in Eq. (2). Value of PCI less than 10 represents low rainfall variability, 11–20 represents moderate rainfall variability, while greater than 20 represents severe rainfall variability

$$PCI_{seasonal} = 25 \times \frac{\sum_{i=1}^3 P_i^2}{\left(\sum_{i=1}^3 P_i\right)^2} \quad (2)$$

where 3 indicates the calculation is for three months (March-April-May), and  $p$  is the rainfall.

### 2.3 Empirical orthogonal functions (EOF)

EOF is a technique used to extract spatial and temporal dominant information from datasets (Yosef et al. 2017), here, rainfall. EOF composes spatial pattern (Eigenvector), Eigenvalue (magnitude of spatial), and temporal time series (principal component/PCs) (Roundy 2015). EOF has widely used in meteorology science to identify climate variability and how it changes with time (Fukuda et al. 2021; Wenhaji Ndomeni et al. 2018), and the equation is presented below.

$$Z(x, y, t) = \sum_{k=1}^N PC(t) \times S(x, y) \quad (3)$$

where  $PC(t)$  denotes time component for  $Z(x, y, t)$  and  $S(x, y)$  represent spatial component for  $Z(x, y, t)$ .  $PC(t)$  is the principal component that tells how the amplitude of each EOF varies with time. In EOF analysis, there is also a concept known as orthogonality, which is interpreted to mean that  $PC1$  and  $PC2$  are not correlated in time and in the same way  $EOF1$  and  $EOF2$  are spatially uncorrelated (Odhiambo et al. 2018). Before analyzing EOF and PC, raw rainfall data was first transformed into normalized anomalies to minimize the impact of high and low values. The main purpose of EOF in this study was to extract spatio-temporal patterns of rainfall in the study area for March-April-May.

#### 2.3.1 Composite analysis

The first step is to divide the ocean-atmosphere circulation variables into two sets of periods of excess and deficit rainfall and then calculate the anomalies by removing the climatology. The composite mean analysis technique is an ideal method for this study to identify linkages patterns

**Table 1** Statistics description of rainfall 1991–2022

| Statistics          | March      | April      | May        | MAM        | Annual     |
|---------------------|------------|------------|------------|------------|------------|
| Mean                | 39.73      | 101.49     | 93.76      | 234.98     | 640.38     |
| Median              | 33.68      | 93.72      | 94.22      | 236.34     | 33.68      |
| Standard deviation  | 16.61      | 28.51      | 20.60      | 41.05      | 16.61      |
| Min                 | 15.66      | 54.85      | 58.56      | 179.05     | 15.66      |
| Max                 | 76.52      | 178.73     | 137.45     | 352.69     | 76.52      |
| Range               | 60.86      | 123.88     | 78.89      | 173.64     | 297.23     |
| Trend               | decreasing | increasing | increasing | increasing | increasing |
| Sig-nificance @0.05 | Non-sig    | Non-sig    | Non-sig    | Non-sig    | Non-sig    |

**Table 2** Shows decadal rainfall variation from climatology (1991–2022)

|            | 1st decadal | 2nd decadal | 3rd decadal | Climatology |
|------------|-------------|-------------|-------------|-------------|
|            | 1991–2000   | 2001–2010   | 2011–2022   | 1991–2022   |
| March      | 39.68       | 40.80       | 38.89       | 39.73       |
| Change (%) | -0.13       | 2.69        | -2.13       |             |
| April      | 93.48       | 101.73      | 107.95      | 101.49      |
| Change (%) | -7.89       | 0.24        | 6.37        |             |
| May        | 95.91       | 86.47       | 98.06       | 93.76       |
| Change (%) | 2.29        | -7.78       | 4.58        |             |
| MAM        | 229.07      | 229.00      | 244.89      | 234.98      |
| Change (%) | -2.52       | -2.54       | 4.22        |             |
| Annual     | 622.35      | 624.31      | 668.79      | 640.38      |
| Change (%) | -2.82       | -2.51       | 4.44        |             |

between atmospheric circulation variables and wet and dry rainfall conditions. It is helpful to reveal the possible underlying physical mechanism by detecting the association between circulation anomaly (e.g., wind fields) and extreme rainfall events and this method is widely applied in such a way including (Alexander & Nyasulu, 2021; Zheleznova & Gushchina, 2015). For this study, the value of PC1 greater than positive unity (+1) is considered extremely wet, while less than negative unity (-1) is extremely dry. Ocean-atmospheric variables that are used for composite mean analyses include sea surface temperature (SST), mean sea surface pressure (SLP), wind field (U&V), vertical velocity (Omega), and potential velocity. The statistical significance of the difference in composite average atmospheric parameters between dry and wet periods was tested using the student t-test method.

## 3 Results and discussion

### 3.1 Rainfall characteristics

The southern and southeastern parts of Ethiopia are experiencing a bimodal rainfall cycle. The first wet season which is the focus of this study is during March-April-May (MAM). The minimum and maximum rainfall during the MAM period ranges from 179 to 352 mm/season. The wettest and driest months during 1991–2022 were April (54.8 to 178 mm/month) and March (15.66 to 76.5 mm/month), respectively. A summary of the statistical rainfall is shown in Table 1.

Table 2 describes the first, second, and third decadal rainfall variation for each month (March, April, May), seasonal MAM, and Annual. The results showed that the MAM and annual rainfall in the third decade (2011–2022) increased significantly by 4.22% and 4.44%, respectively. In addition, rainfall in April and May also increased in the third decade by 6.37% and 4.58%, respectively. The basis for comparison of all decades is climatology (1991–2022).

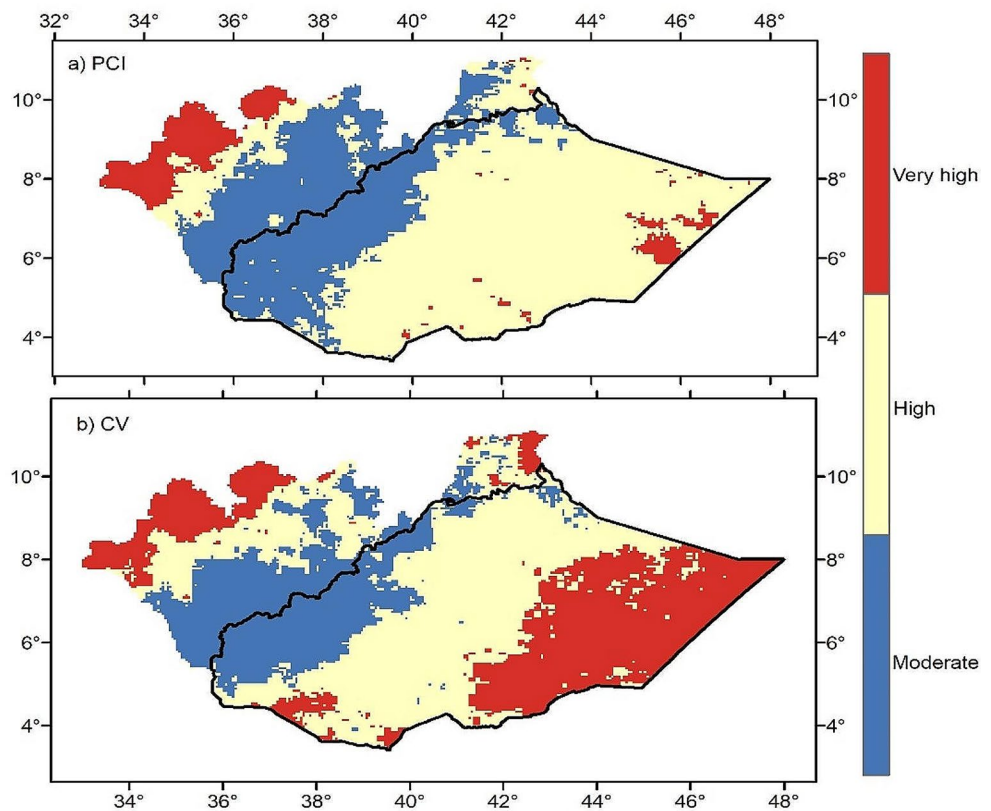
### 3.2 Spatial rainfall variability

Spatial variability in rainfall analysis was performed using the coefficient of variation (CV) and precipitation concentration index (PCI). Rainfall varies more in the east of the region. As shown in Fig. 2, the results for PCI (a) and CV (b) have almost similar spatial patterns. The areas with red color in Fig. 2a) and (b) represent very high rainfall variations, while the yellow color represents high and the blue color indicates areas of moderate rainfall variations. Both methods indicate a moderate to very high level of rainfall variation experienced in the region. This result agreed with the previously studied by (Worku et al. 2022) over the Borona which is a small part of the current study area. As documented by Gebremichael et al. (2014), areas with a high value of CV are vulnerable to drought, and hence, the result of CV in (Fig. 2a) indicates that the eastern parts of the study area are at potential risk of drought.

### 3.3 Dominant mode of EOF for seasonal MAM over the study area

EOF techniques were applied to examine spatial rainfall homogeneity over the study area. Figure 3 displays spatial patterns for the first three leading EOF and corresponding principal components (PCs) for spring (MAM). The variance of the first, second, and third EOF modes are 48.8%, 12.1%, and 6.8% respectively. The three modes account for 67.7% of the entire rainfall variance over the region. The first mode is characterized by dominantly positive loadings

**Fig. 2** Spatial precipitation concentration index (a) and coefficient variation (b) of rainfall variability for MAM during 1991–2022



with stronger signals in the central part of the region. On the other hand, the second EOF2 is characterized by a negative mode in the south and a positive in the north part of the study domain. The variance of the third mode (EOF3) shows that zonal triple pattern which is positive at the western and shifted to negative at the center and then positive dominant mode at the eastern.

The principal component in Fig. 3 shows temporal variation of rainfall that is how rainfall varies with time over the domain of period. For example, PC1 represents more positive signals before 2000, and more negative signals in the middle time after 2000, and has recently shown annual variation with positive and negative significant magnitude. Comparing the three PCs time series with the rainfall anomaly index (Fig. 4), PC1 can capture rainfall patterns well. Thus, PC1 was used to identify extreme wet and dry periods for composite analysis. For composite analysis the value of PC1 and rainfall anomaly index which are both greater than positive (+1) are considered as more extreme wet years whereas less than negative (-1) is extreme dry years.

### 3.4 Diagnosis of extreme wet/dry conditions

Rainfall climatology distribution for the season of MAM and for individual Months of March, April, and May are presented in Fig. 5. Rainfall was decreased zonally from west to east. More rainfall deficit was observed over the

lowland areas of the study domain. In general, the results indicate that the rainfall for each month and season of MAM show a zonally decreasing pattern from west to east, which is consistent with the coefficient of variations (see Fig. 2).

Principal components and standardized anomaly index were used to determine the dry and wet conditions in the spring of 1991–2022. Here, the threshold classification for wet is greater than the unit, while the threshold classification for dry is less than the negative unit and Table 3 presents dry and wet years.

The average rainfall and their anomalies for wet and dry MAM are shown in Fig. 6. More rainfall was observed at the Gamo zone. The wet and dry rainfall anomalies present in (Fig. 6c & d) are the deviation from the climatology of MAM (1991–2022). The study area is characterized by positive rainfall anomalies during wet MAM (c) and negative rainfall anomalies during dry MAM (d). In dry years, rainfall in the region decreased up to 50 mm, while in wet years, it increased up to 120 mm. Rainfall deficits were observed in the southeastern parts including the areas of Afder, Shabelle, Korahe, and Doolo. More rainfall was also observed around the Gamo zone. The hatched areas represent statistically significant change at a 5% significant level.

**Fig. 3** EOF and PCs for MAM rainfall during 1991–2022

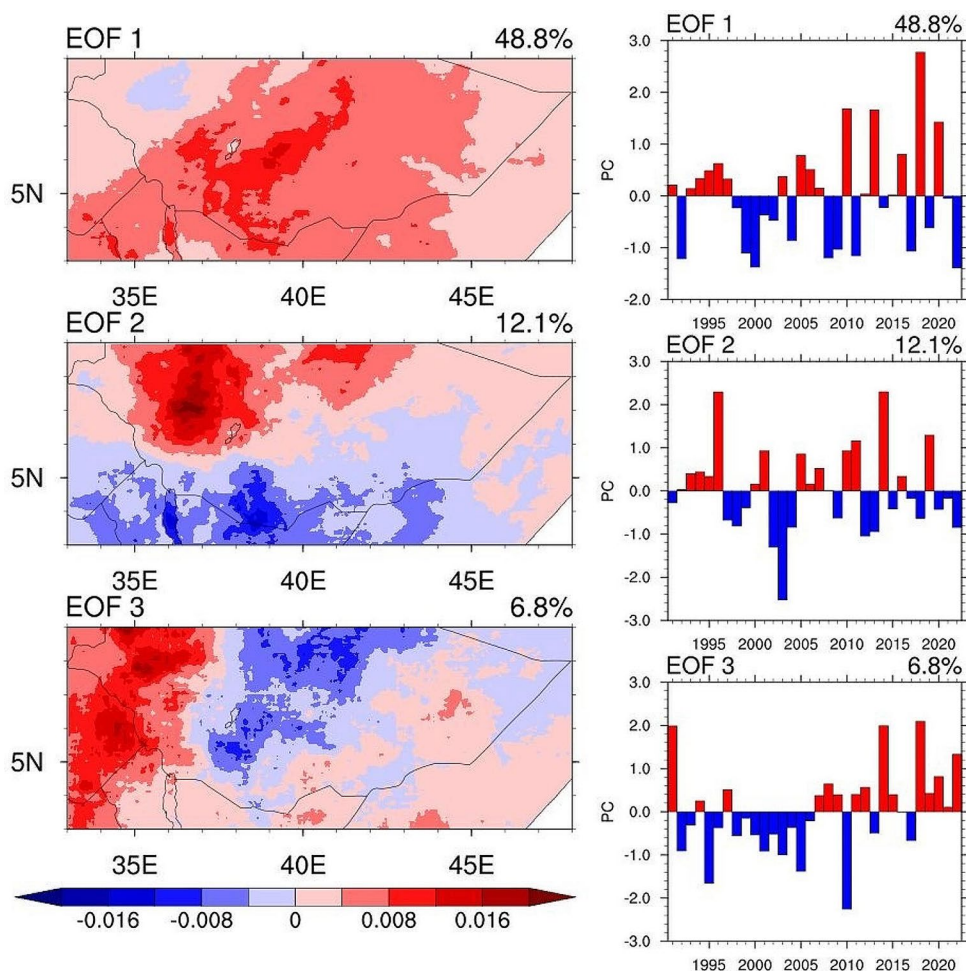
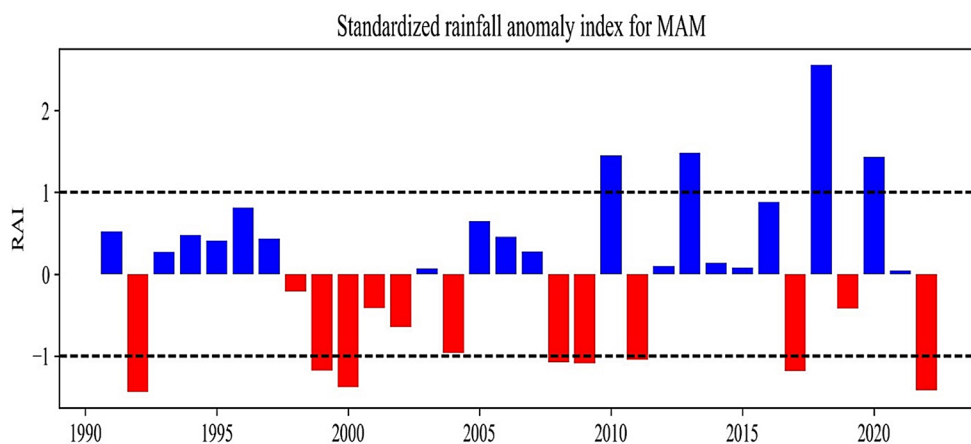


**Fig. 4** Standardized rainfall index, the dashed line indicates extreme wet/dry thresholds



### 3.5 Composites of SST anomalies associating with wet/dry

The effects of sea surface temperature western Indian Ocean on rainfall in the study area were analyzed during wet and dry conditions. As presented in Fig. 7, SST Indian Ocean significantly increased during wet years (Fig. 7a), while declining during drought years (Fig. 7b). It showed positive

and negative anomalies for wet and dry periods respectively. This indicates warming of the SST Indian Ocean is favorable to more precipitation in the study area, while cooling is a deficit. The shaded areas represent statistically significant change between dry and wet periods at 5% significant level.

The El Niño Southern Oscillation (ENSO) is the largest climate signal (Sterl et al. 2007) caused by periodic fluctuations in sea surface temperature in the eastern

**Fig. 5** Rainfall climatology (mm) for MAM (a), March (b), April (c) and May (d) 1991–2022

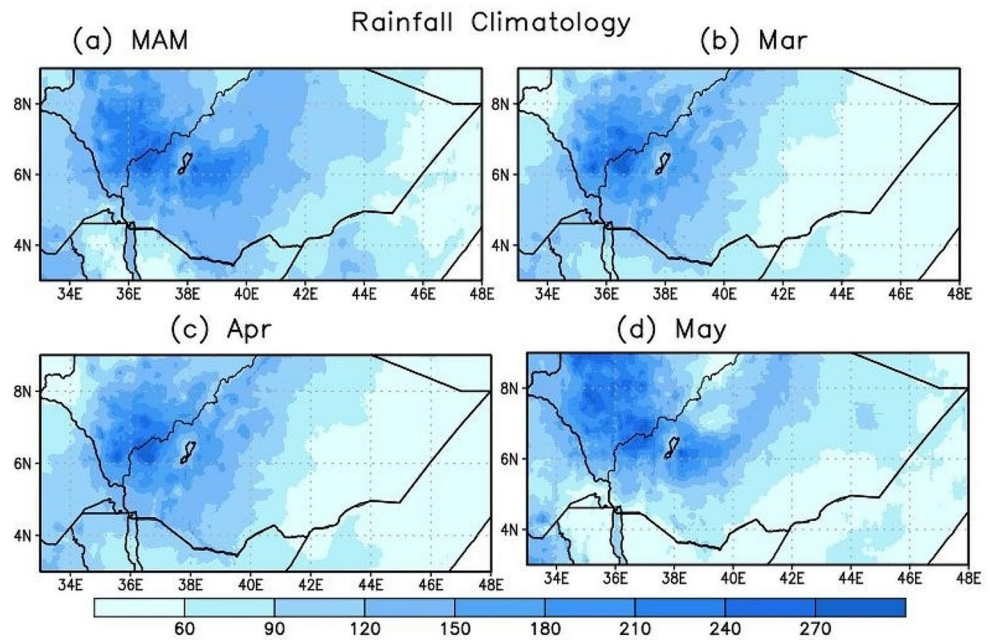


**Table 3** Classification of wet and dry conditions during 1991–2022

| Season | Grade  | Years                                   | PC1         | Occurrence (%) |
|--------|--------|---|-------------|----------------|
| MAM    | Wet    | 2010,2013,2018 and 2020                 | PC > 1      | 12.5           |
|        | Dry    | 1992,1999,2000,2008 2009,2011,2017 2022 | PC < -1     | 25             |
|        | Normal | the rest years                          | -1 ≤ PC ≤ 1 | 62.5           |

convenient measurement of ENSO is the Nino3.4 index (Van Oldenborgh et al. 2021), which is defined as the average SST anomaly in the region of 17° E -120° W, 5° S – 5° N.

To understand the effect of El Niño southern oscillation (ENSO) on local rainfall under the Nino 3.4 index (Trenberth 1997), the La Niña and El Niño periods of MAM were first identified. Table 4 displays all La Niña and El Niño events along with the driest and wettest periods in 1991–2022.

As pointed out in Table 4, La Niña events are linked to five of the driest periods, account for 62.5% of the total,

and western regions of the tropical Pacific Ocean. The

**Fig. 6** Average rainfall (mm) for wet (a) and dry (b) years and their anomalies (c&d). Anomalies are a departure from the 1991–2022 seasonal climatology of MAM. The hatched area represents a statistical significance test at 0.05 (c & d)

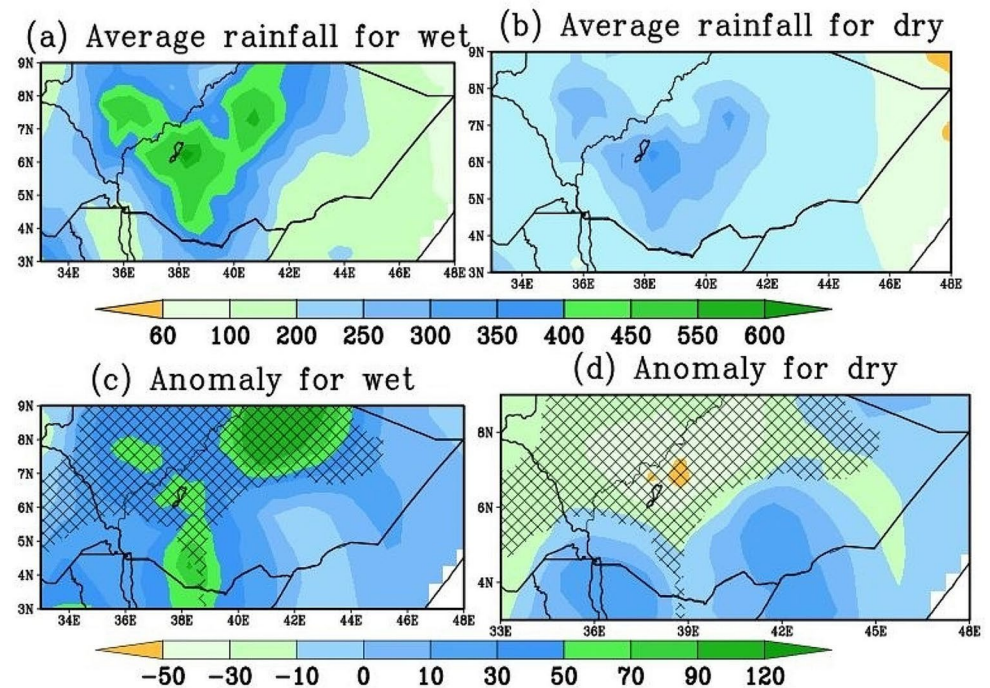




**Fig. 7** Composite of SST Indian Ocean anomaly ( $^{\circ}$ C) during wet (a) and dry (b), (contour interval: 0.1), the box indicates the Indian Ocean. Anomalies are departures from the 1991–2022 base period

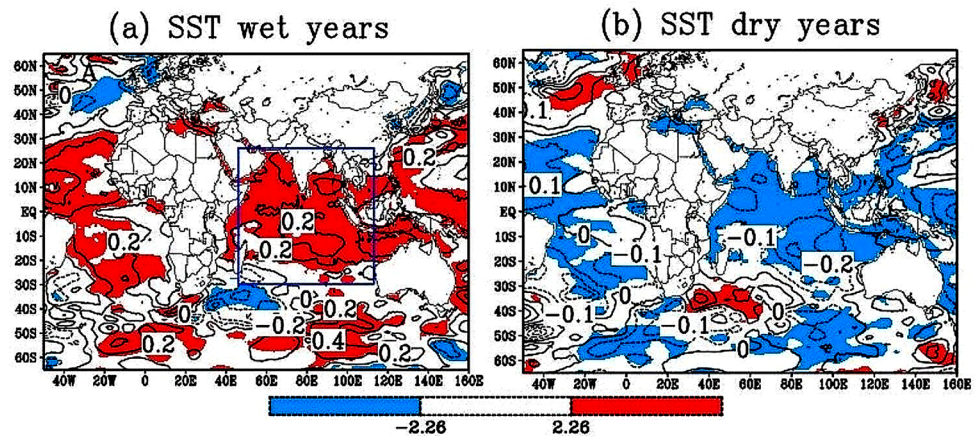


**Table 4** La Niña, El Niño events, the driest and wettest years in 1991–2022

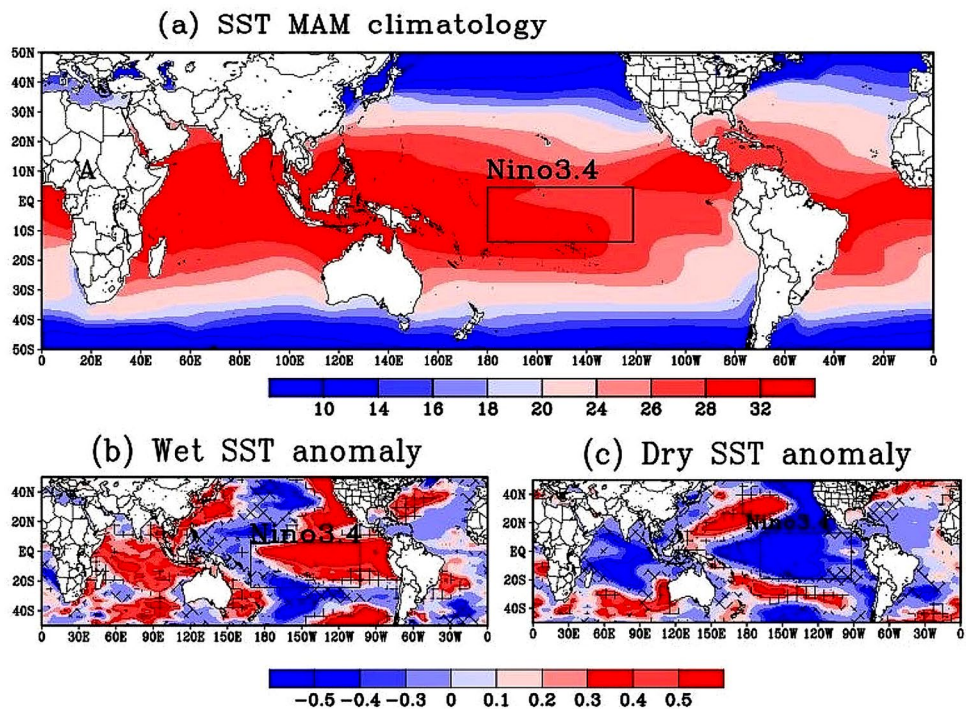
| La Niña years | Dry years | Events  | El Niño years | Wet year | Events  |
|---------------|-----------|---------|---------------|----------|---------|
| 1999          | 1999      | La Niña | 1992          | 2010     | Neutral |
| 2000          | 2000      | La Niña | 1998          | 2013     | Neutral |
| 2008          | 2008      | La Niña | 2015          | 2018     | Neutral |
| 2011          | 2011      | La Niña | 2016          | 2020     | El Niño |
| 2012          | 1992      | El Niño | 2019          |          |         |
| 2018          | 2009      | Neutral |               |          |         |
| 2021          | 2017      | Neutral |               |          |         |
| 2022          | 2022      | La Niña |               |          |         |

while two dry years, namely 2009 and 2017, were occurred during neutral events. On the other hand, with regards to wet years, all but one (2018) coincided with neutral conditions, whereas the year, 2018, coexisted with El Niño. Therefore,

the results suggest a stronger association between La Niña and drought conditions compared to wet periods in the study area during the analyzed period. SST anomaly during the dry and wet periods also displays as shown in Fig. 8.

Figure 9 illustrates the time series bar plots that depicting the Nino3.4 index and the standardized precipitation index (SPI) during the period of MAM. The horizontal lines in the Fig. 9 at positive and negative 0.5 are a thresholds, which are values greater than 0.5 as indicative of El Niño conditions and values less than negative 0.5 La Niña conditions. The values falling between positive and negative 0.5 represent neutral years. This visualization is used to show how El Niño and La Niña events associated/impacted on local rainfall.

**Fig. 8** SST climatology(a), a composite of an anomaly for wet (b) and for dry (c) during MAM 1991–2022



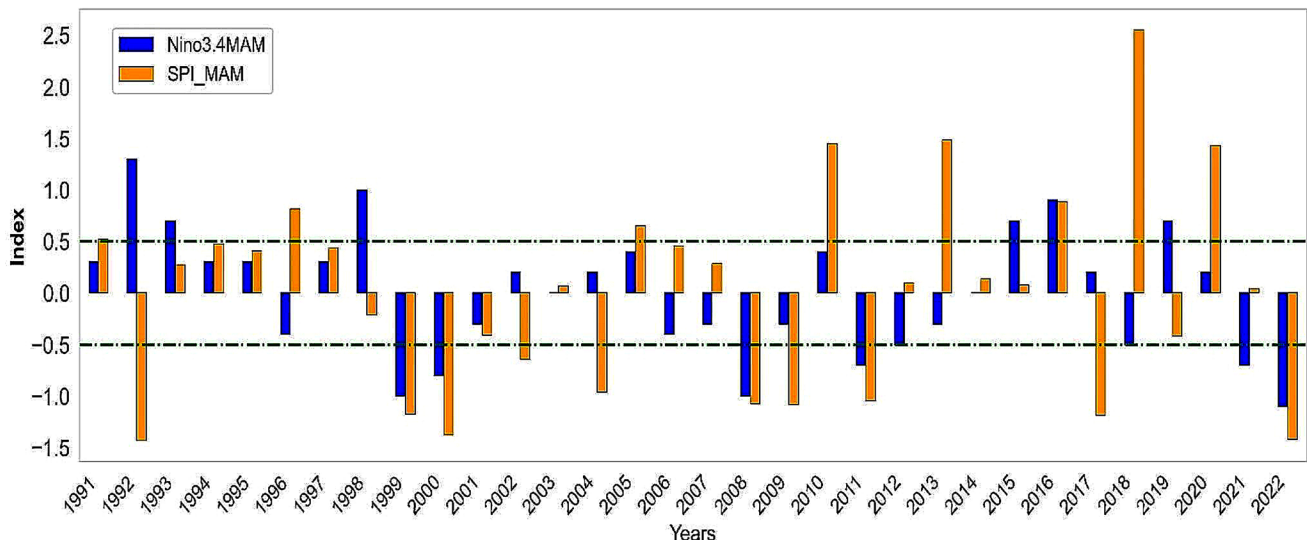
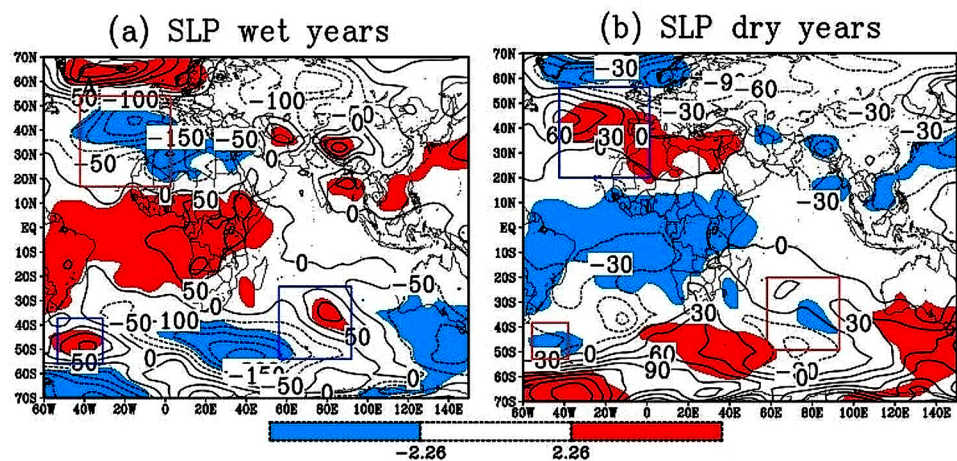


**Fig. 9** SST Nino3.4 index and standardized precipitation index for MAM 1991–2022

**Fig. 10** Composite of pressure anomalies (Pa) (contour interval:10) for Azores, Mascarene, and St. Helena high (marked by boxes) during extreme wet (a) and dry (b). The shaded areas significance test at 0.05 level. Anomalies are departures from the 1991–2022 base period



### 3.6 Composite semi-permanent pressure center anomalies associating with wet/dry

This section demonstrates the influence of the Azores and St. Helena semi-permanent high-pressure center from the north and south Atlantic Ocean, and Mascarene high from the south Indian Ocean on the rainfall of the study area during wet and dry periods. The composite maps present in Fig. 10 for wet (a) and dry (b) years, the pressure centers are also marked by a box. The results showed that the Mascarene and St. Helena high-pressure centers intensified during wet and weakened during the dry periods. Both centers significantly reduced pressure anomalies and changed from positive (during wet) to negative (during dry). In contrast, the Azore's High pressure weakened during wet periods but strengthened during dry periods. In addition, the significant area of the Azores High expands a large area compared to Mascarene and St. Helena High. Further, Azores High has a

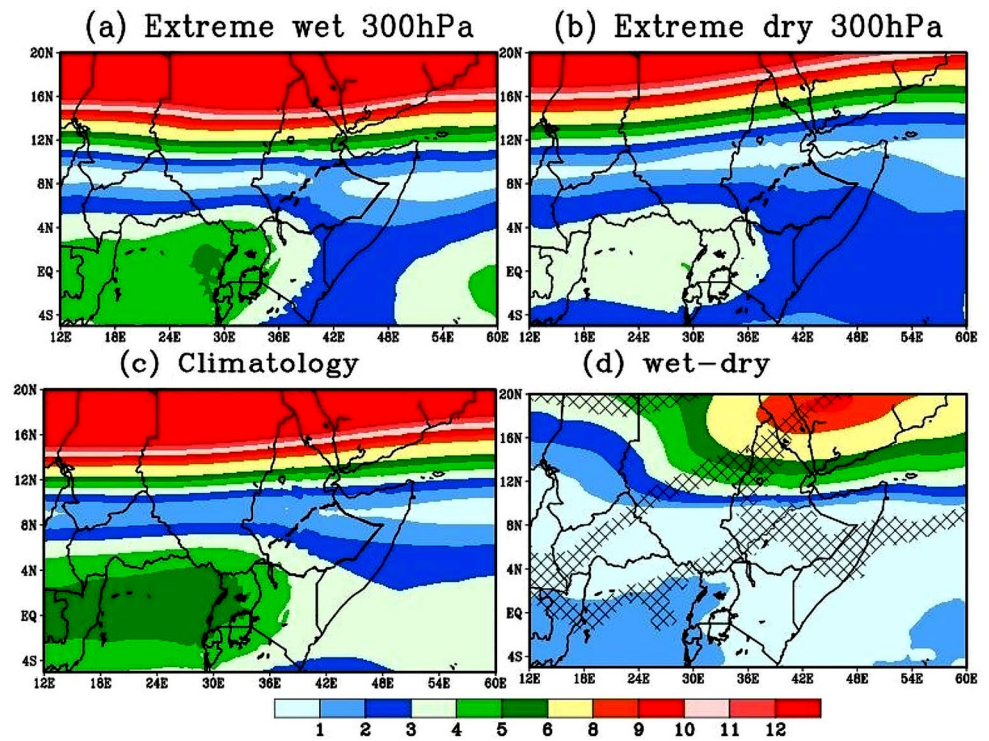
strong negative correlation with rainfall during MAM (the figure not presented here). This means the semi-permanent Azores High has a significant impact on rainfall in the study area. Thus, the intensification of the high pressure in the Azores is associated with drought years, while weakening is associated with extreme wet/floods.

### 3.7 Composites of wind and wind anomaly vectors associating with wet/dry

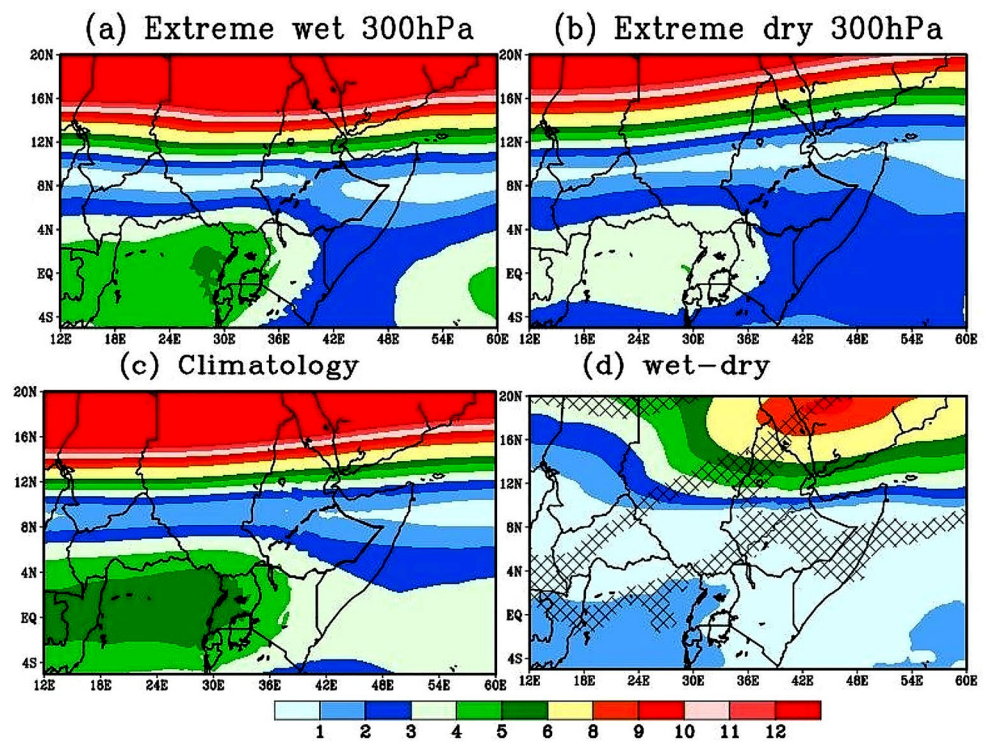
#### 3.7.1 Wind magnitude lower Troposphere (850-hPa)

Figure 11 displays the average wind magnitude for wet (a), dry (b), climatology (c), and the difference between wet and dry periods (d). Weak winds were observed during drought periods, especially in the southeast of the study area, compared to wet periods. The climatology (c) and average wet period (a) wind magnitude showed similar patterns. The

**Fig. 11** Composite of wind magnitude (m/s) at lower troposphere for wet (a), dry (b), climatology (c), and wet-dry (d). Climatology is MAM for 1991–2022



**Fig. 12** Composite of wind magnitude (m/s) upper troposphere (300-hPa) wet (a), dry (b), climatology (c) and wet-dry (d). Climatology is 1991–2022 during March-April-May



wind magnitude outside the study domain near 16° N and 24° E marked by a red box (Fig. 11a) in northern Sudan was remotely shown teleconnection with the wet and dry periods in the study area. It indicates stronger wind associated with more rainfall, while weaker wind deficit of rainfall.

### 3.7.2 Wind magnitude upper Troposphere (300-hPa)

Figure 12 shows the average wind magnitude of extreme wet (a), dry (b), climatology (c), and the difference between wet and dry (d). Dry/drought years were characterized by stronger speeds compared to extremely wet years. Wind

speed was 3 m/s throughout the study area, while in wet conditions, except for a small portion which is the southern part, the wind speed was 2 m/s. As shown in (Fig. 12a & b) the weakening wind speed outside of the study domain that is at South Sudan, Democratic Republic Congo (DRC), and Central Africa Republic (CAR) results in rainfall deficiency/drought in the study area whereas strengthening is bearing above normal rainfall.

### 3.7.3 Wind anomalies vector lower (850-hPa) and upper (300-hPa) Troposphere

Figure 13 presents the wind anomalies vector for wet (a) and dry (b) years. Dry years were characterized by easterly winds over the study area and unusually weaker wind direction than in extreme wet. As indicated in (Fig. 13a), two channels of moisture-carrying air masses enter the study area during extreme wet periods. An air masses from the southern Indian Ocean passed through Kenya into the study area and then deflected eastward. The second channel of air masses also from the Congo Forest Basin travelled at central Sudan and then deflected to the study area. This air masses are warmer and moist with stronger speed and thus, likely contribute to above-normal rainfall over the study area. On the other hand, the weakening of the air masses from the Congo Forest basin can cause extreme rainfall deficiency in the study area. Generally, the result showed that higher wind speeds that come from the Congo basin are associating with

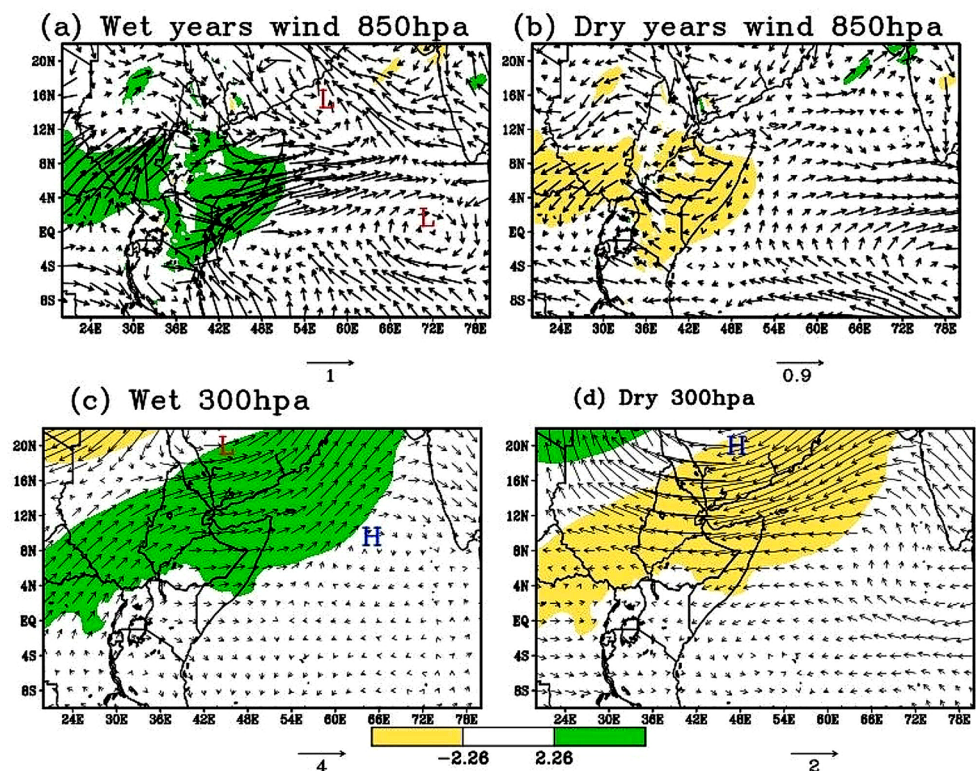
surplus rainfall whereas the reverse of this causes droughts over the study area.

The wind anomalies for the upper troposphere (300-hPa) during wet (c) and dry periods (d) are characterized by westerly and easterly winds respectively. The magnitude of wind anomaly vectors for dry years was smaller than that of wet periods. Except for the southern end known as “Borona”, the entire study domain area is a statistically significant change at a 95% confidence level.

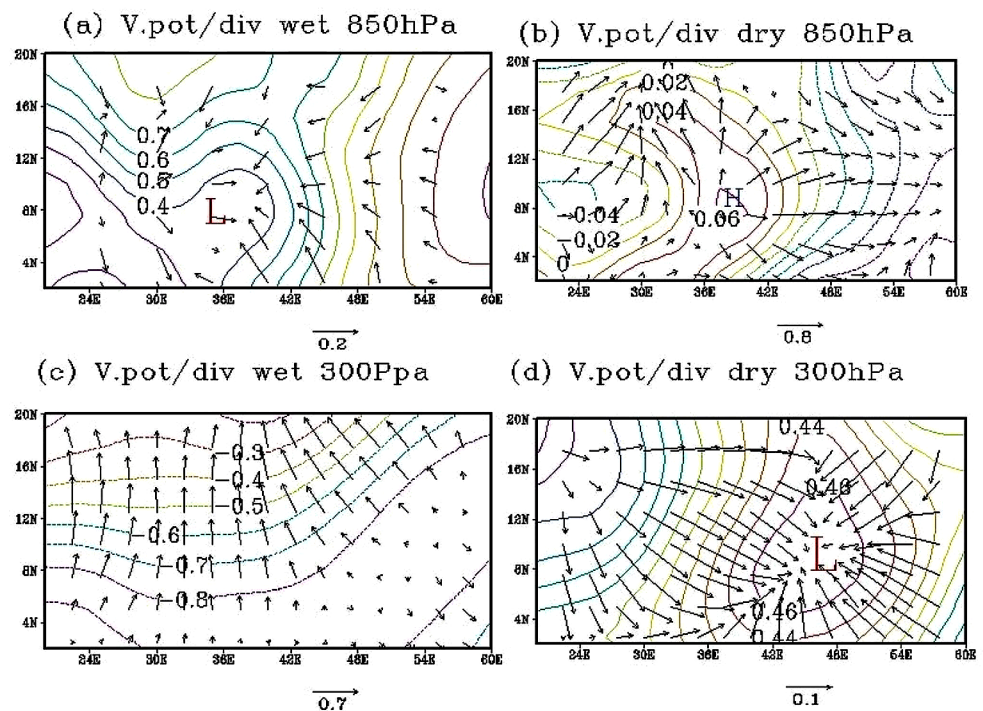
### 3.8 Composite of velocity potential anomaly/divergent associating with wet/dry

Figure 14 shows composite velocity potential anomaly/divergence at lower (850-hPa) and upper (300-hPa) troposphere during extreme wet and dry years. In the study area, during the wet period, positive velocity potential anomalies and wind convergence at lower (Fig. 14a) and negative velocity potential anomalies and wind divergence at the upper troposphere (Fig. 14c) were observed. The convergence is centered around 8° N and 38° E. Wind convergence in the lower troposphere favors the upward movement of the air and may cause higher than normal rainfall. Conversely, drought periods are characterized by negative velocity potential anomalies and wind divergence in the lower troposphere (Fig. 14b), while positive velocity potential anomalies and wind converge in the upper troposphere (Fig. 14d). This results agreed with previous study (Ogwang et al.

**Fig. 13** Composite of wind vector anomalies (m/s) at lower (850-hPa) and upper (300-hPa) troposphere, the shaded area significance at 0.05 level. Anomalies are departures from the 1991–2022 base period



**Fig. 14** Composite maps of velocity potential anomalies/v. pot (contour lines) (unit:  $\times 10^6 \text{ m}^2\text{s}^{-1}$ ). Vectors (arrows) divergence/convergence. Anomalies are departures from the 1991–2022 base period



2012). The centers of convergence and divergence for the lower (850-hPa) dry period and upper (300-hPa) are around  $8^\circ \text{ N}$  and  $38^\circ \text{ E}$ ,  $8^\circ \text{ N}$  and  $48^\circ \text{ E}$  respectively.

**3.9 Composite vertical velocity anomaly associating with wet/dry season**

Vertical velocity( $\omega$ ) anomaly profile composite associated with wet and dry MAM over the latitudinal range at fixed  $40^\circ \text{ E}$  was investigated for wet and dry years. Figure 15 illustrates vertical velocity anomalies for wet (a) and dry years (b). During the wet period, the result reveals strong negative values observed at the lower troposphere that is from the surface to 700-hPa pressure level and then shifted to strong positive toward 200-hPa pressure height. This is a favorable condition for strong vertical ascending motion, then, enhances cloud and rainfall formation. In contrast, the positive vertical velocity anomaly observed at lower and negative at upper troposphere in the dry periods is conducive for air subsidence which leads to drought events. Similar results were found by (Ngoma et al. 2021). In addition, the result indicated that the magnitude of the vertical velocity anomaly in the extreme rainy or flood season is greater than in the dry season. Strong positive vertical velocities in the lower atmosphere were associated with drought, while strong negatives caused more rainfall. The negative and positive values of  $\omega$  in the lower troposphere indicate upward and downward motion respectively.

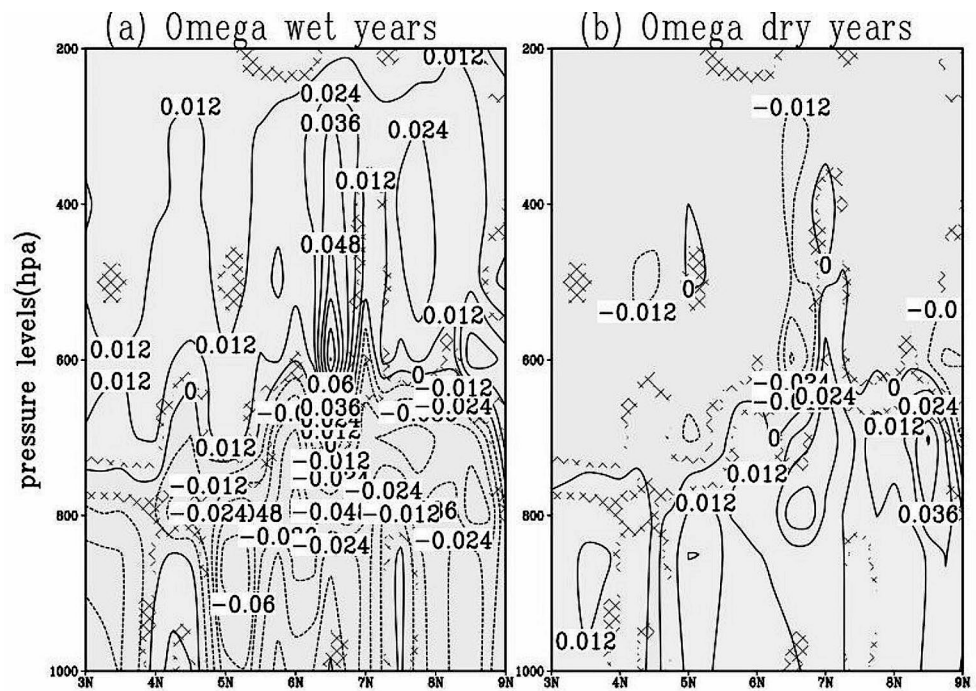
**4 Summary and conclusion**

This study investigated atmospheric circulation anomaly patterns associating with seasonal rainfall variability for long rain season (March-April-May) over southern and south-eastern Ethiopia starting from 1991 to 2022 time period. CHIRPS rainfall products selected for rainfall variability assessment .

According to the research results, the rainfall in this area has undergone significant variation, and the degree of variation has increased towards the eastern part of the study area. EOF1 shows positive loadings throughout the entire area and accounts for 48.8% of variation. The corresponding EOF1 is PC1 which reveals temporal variation and, in this study, it was used to identify extreme wet and dry periods. Eight severe dry years (1992, 1999, 2000, 2008, 2009, 2011, 2017, and 2022) and four extreme wet years 2010, 2013, 2018, and 2020 were identified in the period of 1991–2022.

Various weather systems have been attributed to fluctuation of rainfall during March-April-May. Therefore, Indian Ocean Sea surface temperatures, Nino index 3.4, semi-permanent sea level pressure, wind fields, vertical velocity, and potential velocity data have used to characterize the circulation anomalies related to the dry and wet conditions. The composite analysis revealed a significant increase in western Indian Ocean Sea surface temperature during wet years, and Mascarene and St. Helena semi-permanent high-pressure centers showed intensification, while Azores high pressure weakened significantly. During the

**Fig. 15** Composite of vertical velocity anomaly(omega), contour interval 0.012, units, (Pas-1), hatched area significance test at 0.05. Anomalies are departures from the 1991–2022 base period



rainy season, negative vertical velocity anomalies in the lower troposphere and positive ones in the upper troposphere were observed, potentially enhancing rainfall. In contrast, during drought years, vertical velocity anomalies were positive in the lower troposphere and negative in the upper troposphere, supporting the suppression of rainfall by sinking air motions. The findings also showed that 62.5% of the dry years are associating with La Niña events, while the most of wet periods occurred during neutral periods. During periods of extreme wet, wind directions in the lower troposphere (850-hPa) blow from southwestern Sudan to central Sudan and then turned towards the study area. Likewise, strong winds (300-hPa) in the upper troposphere blow from the southwest and are completely diverted to the westerlies in the study area. This wind may have brought moisture to the study area to increasing rainfall above normal levels. Strong wind anomalies were observed during wet periods compare to drought years at the lower troposphere. During dry periods the upper and lower troposphere were opposite to those during wet periods, resulting in below normal rainfall in the region. The research results in wet periods, were also characterized by positive velocity potential anomalies and convergence at lower (850-hPa) and negative potential velocity anomaly and divergence at the upper (300-hPa) troposphere. The reverse characteristics of the wet period was also true for dry periods.

In conclusion, the study highlights that the magnitude of the winds in the Congo Forest Basin at 850-hPa, the semi-permanent pressure centers in the Azores, the SST in the Indian Ocean, the Nino index of 3.4 and the vertical velocity

are the predictors that should be taken into account in rainfall forecasting operations.

**Acknowledgements** The first author would like to thank the Chinese Government Scholarship Committee (CSC) for giving me an educational opportunity at the Institute of Atmospheric Physics at the University of the Chinese Academy of Sciences (UCAS). He also thanks Climate Hazards Group InfraRed Precipitation with Station data (CHIRPS), the European Center for Medium-Range Weather Prediction (ECWMF), and National Centers for Environmental Prediction (NCEP/NCAR) for providing me with rainfall and atmospheric data respectively.

**Author contributions** All authors contributed to the conception and design of the study. Material preparation, data collection and analysis were performed by “Tewelde Berihu, Wen Chen, and Lin Wang”. The first draft of the manuscript was written by “Tewelde Berihu”, and all authors commented on previous versions of the manuscript, and then all authors read and approved the final manuscript.

**Funding statement** This study is supported by the National Natural Science Foundation of China Grants 42230605 and 42175041, the International Partnership Program of the Chinese Academy of Sciences for Future Network (060GJHZ2022104FN), and the Basic Scientific Program of the Institute of Atmospheric Physics, Chinese Academy of Science during the 14th Five Year Plan period.

**Data availability** No datasets were generated or analysed during the current study.

## Declarations

**Competing interests** The authors declare no competing interests.

## References

- Abegaz WB (2020) Rainfall Variability and trends over Central Ethiopia. *Int J Environ Sci Nat Resour* 24(4). <https://doi.org/10.19080/ijesnr.2020.24.556144>
- Adnew M, Bewket W, Amha Y (2022) Evaluating performance of 20 global and quasi-global precipitation products in representing drought events in Ethiopia I: visual and correlation analysis. *Weather Clim Extremes* 35:100416. <https://doi.org/10.1016/j.wace.2022.100416>
- AL-Shamarti HKA (2016) The variation of Annual Precipitation and Precipitation Concentration Index of Iraq. *IOSR J Appl Phys* 08(04):36–44. <https://doi.org/10.9790/4861-0804033644>
- Alhamshry A, Fenta AA, Yasuda H, Shimizu K (2020) Seasonal Rainfall variability in Ethiopia and its long-term link to Global Sea Surface temperatures. <https://doi.org/10.3390/w12010055>. January
- Ayalew M (2020) The role of Rainfall amount and distribution on Agriculture Systems and Crop Cropping systems of different agro-ecological regions of Ethiopia: a review. *Int J Res Agric Forestry* 7(5):26. <http://www.yieldgap.org/>
- Barua S, Muttill N, Ng AWM, Perera BJC (2013) Rainfall trend and its implications for water resource management within the Yarra River catchment, Australia. *Hydrol Process* 27(12):1727–1738. <https://doi.org/10.1002/hyp.9311>
- Bayable G, Amare G, Alemu G, Gashaw T (2021) Spatiotemporal variability and trends of rainfall and its association with Pacific Ocean Sea surface temperature in West Harerge Zone, Eastern Ethiopia. *Environ Syst Res*. <https://doi.org/10.1186/s40068-020-00216-y>
- Beheshti M, Heidari A, Saghafian B (2019) Susceptibility of hydro-power generation to climate change: Karun III Dam case study. *Water (Switzerland)* 11(5). <https://doi.org/10.3390/w11051025>
- Billi P, Alemu YT, Ciampalini R (2015) Increased frequency of flash floods in dire Dawa, Ethiopia: change in rainfall intensity or human impact? *Nat Hazards* 76(2):1373–1394. <https://doi.org/10.1007/s11069-014-1554-0>
- Cheung WH, Senay B, Singh A (2008) Trends Spat Distribution Annual Seasonal Rainfall Ethiopia 1734(March):1723–1734. <https://doi.org/10.1002/joc.1623>
- Degefu MA, Tadesse Y, Bewket W (2021) Spatiotemporal variability and trends of drought episode in southeastern Ethiopia Spatio-temporal variability and trends of drought episode in. *Phys Geogr* 00(00):1–28. <https://doi.org/10.1080/02723646.2021.1930654>
- Dinku T, Funk C, Peterson P, Maidment R, Tadesse T, Gadain H, Ceccati P (2018) Validation of the CHIRPS satellite rainfall estimates over eastern Africa. *Q J R Meteorol Soc* 144(June 2017):292–312. <https://doi.org/10.1002/qj.3244>
- Diro GT, Grimes DIF, Black E (2011) Teleconnections between Ethiopian summer rainfall and sea surface temperature: part I-observation and modelling. *Clim Dyn* 37(1):103–119. <https://doi.org/10.1007/s00382-010-0837-8>
- Finney DL, Woodhams BJ, Marsham JH, Walker DP, Jackson LS, Hardy S, Birch CE (2020) The effect of westerlies on East African rainfall and the associated role of tropical cyclones and the Madden – Julian Oscillation. *Quarterly Journal of the Royal Meteorological Society, December 2019*, 647–664. <https://doi.org/10.1002/qj.3698>
- Fu J, Liu M, Wang R, Wang Y, Zhao S (2022) Possible Impact of Boreal Winter siberian high on ENSO Development in the following year. *Front Earth Sci* 10(April):1–9. <https://doi.org/10.3389/feart.2022.885846>
- Fukuda Y, Watanabe M, Jin FF (2021) Mode of Precipitation Variability generated by Coupling of ENSO with Seasonal Cycle in the Tropical Pacific. *Geophys Res Lett* 48(16). <https://doi.org/10.1029/2021GL095204>
- Gebremicael TG, Mohamed YA, Van Der Zaag P, Berhe AG, Haile GG, Hagos EY, Hagos MK (2017) Comparison and validation of eight satellite rainfall products over the rugged topography of Tekeze-Atbara Basin at different spatial and 2 temporal scales. *Hydrol Earth Syst Sci*. <https://doi.org/10.5194/hess-2017-504>
- Gebremichael A, Quraishi S, Mamo G (2014) Analysis of Seasonal Rainfall Variability for Agricultural Water Resource Management in Southern Region, Ethiopia Inter tropical convergence zone length of growing period. *J Nat Sci Res* 4(11):56–80
- Gleixner S, Keenlyside N, Viste E, Korecha D (2017) The El Niño effect on Ethiopian summer rainfall. *Clim Dyn* 49(5–6):1865–1883. <https://doi.org/10.1007/s00382-016-3421-z>
- Gummedi S, Rao KPC, Seid J, Legesse G, Kadiyala MDM, Takele R, Amede T, Whitbread A (2018) Spatio-temporal variability and trends of precipitation and extreme rainfall events in Ethiopia in 1980–2010. *Theoret Appl Climatol* 134(3–4):1315–1328. <https://doi.org/10.1007/s00704-017-2340-1>
- Haile AT, Kusters K, Wagesho N (2013) Loss and damage from flooding in the Gambela region, Ethiopia. *Int J Global Warming* 5(4):483–497. <https://doi.org/10.1504/IJGW.2013.057290>
- Hua W, Zhou L, Nicholson SE, Chen H, Qin M (2019) Assessing reanalysis data for understanding rainfall climatology and variability over Central Equatorial Africa. *Clim Dyn* 53(1–2):651–669. <https://doi.org/10.1007/s00382-018-04604-0>
- IGAD (2017) *Report on Historical Climate Baseline Statistics for East and West Hararge, Ethiopia Vol 2*. 2, 33
- Jayakumar SDKV (2021) A study on copula – based bivariate and trivariate drought assessment in Godavari River basin and the teleconnection of drought with large – scale climate indices. *Theoret Appl Climatol* 1335–1353. <https://doi.org/10.1007/s00704-021-03792-w>
- Kalnay E, Kanamitsu M, Kistler R, Collins W, Deaven D, Gandin L, Iredell M, Saha S, White G, Woollen J, Zhu Y, Chelliah M, Ebisuzaki W, Higgins W, Janowiak J, Mo KC, Ropelewski C, Wang J, Leetmaa A, Joseph D (1996) The NCEP/NCAR 40-year reanalysis project. In *Bulletin of the American Meteorological Society* (Vol. 77, Issue 3, pp. 437–471). [https://doi.org/10.1175/1520-0477\(1996\)077%3C0437:TNYRP%3E2.0.CO;2](https://doi.org/10.1175/1520-0477(1996)077%3C0437:TNYRP%3E2.0.CO;2)
- Kebacho LL (2022) Large – scale circulations associated with recent interannual variability of the short rains over East Africa. *Meteorol Atmos Phys* 134(1):1–19. <https://doi.org/10.1007/s00703-021-00846-6>
- Legese Jima W, Korecha D, Tur K (2019) Impact of Climate Change on Seasonal Rainfall patterns over Bale Highlands, Southeastern Ethiopia. *Int J Environ Chem* 3(2):84. <https://doi.org/10.11648/j.ijec.20190302.15>
- Link L, Sea G, Temperatures S (2020) Seasonal Rainfall variability in Ethiopia and its. *Water*, 1–19
- Manatsa D, Chingombe W, Matarira CH (2008) The impact of the positive Indian Ocean dipole on Zimbabwe droughts Tropical climate is understood to be dominated by. *International Journal of Climatology*, 2029(March 2008), 2011–2029. <https://doi.org/10.1002/joc>
- Manjowe M, Mushore TD, Gwenzi J, Mutasa C, Matandirotya E, Mashonjowa E (2018) Circulation mechanisms responsible for wet or dry summers over Zimbabwe. *AIMS Environ Sci* 5(3):154–172. <https://doi.org/10.3934/ENVIROSCI.2018.3.154>
- Matewos T, Tefera T (2020) Local level rainfall and temperature variability in drought-prone districts of rural Sidama, central rift valley region of Ethiopia. *Phys Geogr* 41(1):36–53. <https://doi.org/10.1080/02723646.2019.1625850>
- Mekonen AA, Berlie AB, Ferede MB (2020) Spatial and temporal drought incidence analysis in the northeastern highlands of Ethiopia. *Geoenvironmental Disasters* 7(1). <https://doi.org/10.1186/s40677-020-0146-4>

- Mekonnen Y (2020) Causes and effects of Drought in Northern Parts of Ethiopia. *Civil Environ Res*. <https://doi.org/10.7176/ceer/12-3-04>
- Mekonnen Z, Kassa H, Woldeamanuel T, Asfaw Z (2018) Analysis of observed and perceived climate change and variability in Arsi Negele District, Ethiopia. *Environ Dev Sustain* 20(3):1191–1212. <https://doi.org/10.1007/s10668-017-9934-8>
- Ngoma H, Wen W, Ayugi B, Karim R, Makula EK (2021) Mechanisms associated with September to November (SON) rainfall over Uganda during the recent decades. *Geogr Pannonica* 25(1):10–23. <https://doi.org/10.5937/gp25-29932>
- Nicholson SE (2018) The ITCZ and the seasonal cycle over equatorial Africa. *Bull Am Meteorol Soc* 99(2):337–348. <https://doi.org/10.1175/BAMS-D-16-0287.1>
- Odhiambo B, Guirong A, Victor T, Mafuru KB (2018) Circulations Associated with Variations in Boreal Spring Rainfall over Kenya. *Earth Systems and Environment*, 0123456789. <https://doi.org/10.1007/s41748-018-0074-6>
- Ogwang BA, Guirong T, Haishan C (eds) (2012) (Droughts) Experienced in the Years. *Pakistan Journal of Meteorology*, 9(17), 11–24
- Oliver JE (1980) M ONTH LY PRECIPITATION DISTRIBUTION: a COMPARATIVE INDEX. *Prof Geogr* 32(3):300–309
- Patil KR, Doi T (n.d.). Predicting extreme floods and droughts in East Africa using a deep learning approach. *Clim Atmospheric Sci*, 1–8. <https://doi.org/10.1038/s41612-023-00435-x>
- Raveh-Rubin S, Wernli H (2015) Large-scale wind and precipitation extremes in the Mediterranean: a climatological analysis for 1979–2012. *Q J R Meteorol Soc* 141(691):2404–2417. <https://doi.org/10.1002/qj.2531>
- Roundy PE (2015) On the interpretation of EOF analysis of ENSO, atmospheric Kelvin waves, and the MJO. *J Clim* 28(3):1148–1165. <https://doi.org/10.1175/JCLI-D-14-00398.1>
- Segele ZT, Lamb J, Leslie LM (2009) Large-scale atmospheric circulation and global sea surface temperature associations with Horn of Africa June – September rainfall. *INTERNATIONAL JOURNAL OF CLIMATOLOGY*, 1100(December 2008), 1075–1100. <https://doi.org/10.1002/joc.1751>
- Senbeta aF (2009) Climate Change Impact on Livelihood, Vulnerability and Coping Mechanisms: A Case Study of West-Arsi Zone, Ethiopia. *Lund University International Master's Programme in Environmental Studies and Sustainability Science*, MSc, 54
- Seyoum A, Ali SN, Paper WW (2015) *Ethiopia: An agrarian economy in transition WIDER Working Paper 2015 / 154 Ethiopia — an agrarian economy in transition Yared Seid, 1 Alemayehu Seyoum Taffesse, 2 and Seid Nuru Ali 3*
- Silva TRBF, Santos CAC, dos, Silva DJF, Santos CAG, da Silva RM, de Brito JIB (2022) Climate indices-based analysis of Rainfall Spatiotemporal variability in Pernambuco State, Brazil. *Water (Switzerland)* 14(14):1–26. <https://doi.org/10.3390/w14142190>
- Sterl A, van Oldenborgh GJ, Hazeleger W, Burgers G (2007) On the robustness of ENSO teleconnections. *Clim Dyn* 29(5):469–485. <https://doi.org/10.1007/s00382-007-0251-z>
- Teshome A, Lupi A (2018) Determinants of Agricultural Gross Domestic product in Ethiopia. *Www Arcjournals Org Int J Res Stud Agricultural Sci* 4(2):2454–6224. <https://doi.org/10.20431/2454-6224.0402002>
- Trenberth KE (1997) The definition of El Niño. *Bull Am Meteorol Soc* 78(12):2771–2777. [https://doi.org/10.1175/1520-0477\(1997\)078%3C2771:TDOENO%3E2.0.CO;2](https://doi.org/10.1175/1520-0477(1997)078%3C2771:TDOENO%3E2.0.CO;2)
- Van Oldenborgh GJ, Hendon H, Stockdale T, L'Heureux M, De Perez C, Singh E, R., Van Aalst M (2021) Defining El Niño indices in a warming climate. *Environ Res Lett* 16(4). <https://doi.org/10.1088/1748-9326/abe9ed>
- Viste E, Korecha D, Sorteberg A (2013) Recent drought and precipitation tendencies in Ethiopia. 535–551. <https://doi.org/10.1007/s00704-012-0746-3>
- Weldegerima TM, Birhanu BS, Zeleke TT (2023) Zoning and agro-climatic characterization of hotspots in the Tana-Beles sub-basin – Ethiopia. *Afr J Agric Res* 19(4):455–465. <https://doi.org/10.5897/AJAR2021.15613>
- Wenhaji Ndomeni C, Cattani E, Merino A, Levizzani V (2018) An observational study of the variability of east African rainfall with respect to sea surface temperature and soil moisture. *Q J R Meteorol Soc* 144(January):384–404. <https://doi.org/10.1002/qj.3255>
- Worku MA, Feyisa GL, Beketie KT, Garbolino E (2022) Rainfall variability and trends in the Borana zone of southern Ethiopia. *J Water Clim Change* 13(8):3132–3151. <https://doi.org/10.2166/wcc.2022.173>
- Yosef G, Alpert P, Price C, Rotenberg E, Yakir D (2017) Using EOF analysis over a large area for assessing the climate impact of small-scale afforestation in a semiarid region. *J Appl Meteorol Climatology* 56(9):2545–2559. <https://doi.org/10.1175/JAMC-D-16-0253.1>
- Zhang K, Yao Y, Qian X, Wang J (2019) Various characteristics of precipitation concentration index and its cause analysis in China between 1960 and 2016. *Int J Climatol* 39(12):4648–4658. <https://doi.org/10.1002/joc.6092>

**Publisher's Note** Springer Nature remains neutral with regard to jurisdictional claims in published maps and institutional affiliations.

Springer Nature or its licensor (e.g. a society or other partner) holds exclusive rights to this article under a publishing agreement with the author(s) or other rightsholder(s); author self-archiving of the accepted manuscript version of this article is solely governed by the terms of such publishing agreement and applicable law.